Supplementary Information (SI) for Nanoscale.

ELECTRONIC SUPPORTING INFORMATION

Functionalization of Three-Dimensional Epitaxial Graphene with Metal Nanoparticles

Emanuele Pompei,[1] Ylea Vlamidis,[1,2] Letizia Ferbel,[1] Valentina Zannier,[1] Silvia Rubini,[3] Daniel Arenas Esteban,[4,5] Sara Bals,[4,5] Carmela Marinelli,[2] Georg Pfusterschmied,[6] Markus Leitgeb,[6] Ulrich Schmid,[6] Stefan Heun,[1] and Stefano Veronesi[1]

[1]*NEST, Istituto Nanoscience-CNR and Scuola Normale Superiore, Piazza S. Silvestro 12, 56127, Pisa, Italy*

[2]*Department of Physical Science, Earth, and Environment, University of Siena, Via Roma 56, 53100, Siena, Italy*

[3]*Istituto Officina dei Materiali CNR, Laboratorio TASC, Area Science Park – S S 14, km 163.5, 34012 Trieste, Italy*

[4]*EMAT, University of Antwerp, Groenenborgerlaan 171, B-2020, Antwerp, Belgium*

[5]*Nanolab Centre of Excellence, Groenenborgerlaan 171, B-2020, Antwerp, Belgium*

[6]*Institute of Sensor and Actuator Systems, TU Wien, 1040, Vienna, Austria*

PRISTINE THREE-DIMENSIONAL GRAPHENE

The fabricated 3DG samples were extensively characterized. Scanning Tunneling Microscopy confirmed the presence of graphene on the top surface of the porous material, see Fig. S1.

The quality of the grown graphene was analyzed via Raman spectroscopy. The graphene 2D peak (Fig. S2a) can be fitted with a single Lorentzian curve, indicating the presence of monolayer graphene [1], consistent with the 2D/G intensity ratio of about 1.6. The D/G intensity ratio is ~ 4.5, suggesting a low density of defects (the estimated average distance between defects is ~ 20 nm [2]). From the distribution of the positions of G peak vs. 2D peak (shown in Fig. S2b) we estimated a compressive strain of $\sim 0.6\%$ and a slight n-type doping of the graphene sheet [3]. All Raman spectroscopy analysis performed here is consistent with that reported in Ref. [4].

The morphology of 3DG was investigated both via High-Angle Annular Dark-Field Scanning Transmission Electron Microscopy (HAADF-STEM) and Scanning Electron Microscopy (SEM). From HAADF-STEM measurements we observed an average pore transverse dimension of (149 ± 48) nm (neglecting all cavities smaller than 30nm). Through SEM, both the sample surface and the cross-section (after cleaving the sample with a diamond tip) were investigated. From SEM measurements we determined an average pore transverse dimension of (166 ± 20) nm, consistent with the HAADF-STEM measurement, and an average distance between pores of (180 ± 29) nm. Due to the larger set of SEM measurements taken into account for extracting these values, their relative errors are lower compared to those from HAADF-STEM. The pore morphology is consistent with that shown in Ref. [4] and resulted in a surface area 200 times larger compared to a flat graphene sample. The average depth of the porous region, extracted from SEM measurements performed on different samples, is (18.1 ± 0.3) μm (SEM images are shown in Fig. S3).

All characterization measurements performed here yielded consistent results with those reported in Ref. [4].

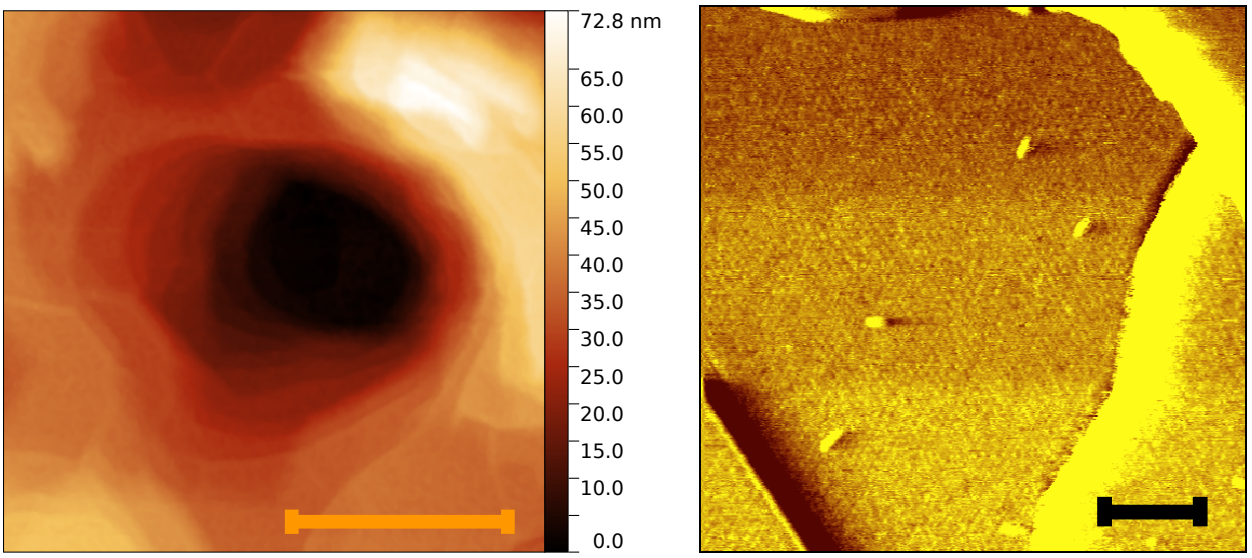

(a)

(b)

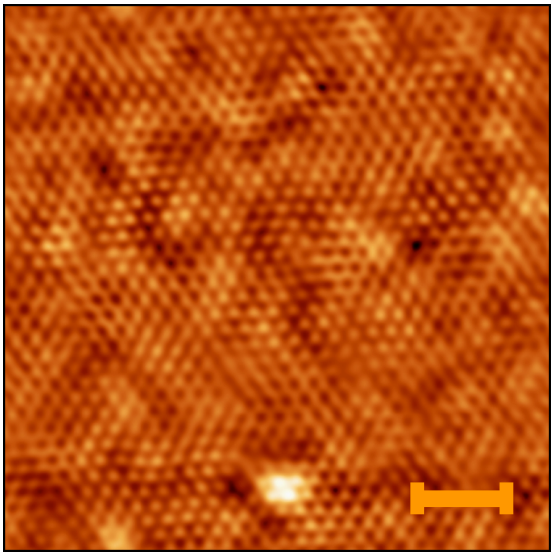

(c)

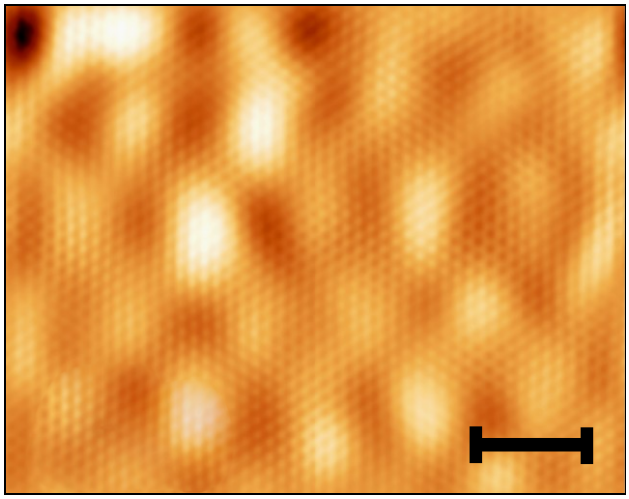

(d)

FIG. S1. (a) 500×500 nm^2 STM image (acquired at V_{bias} = 2 V and I = 0.3 nA) showing the structure of a pore of 3DG. The scale bar indicates 200 nm. (b) 100×100 nm^2 STM image of a 3DG sample (acquired at V_{bias} = 1 V and I = 0.8 nA) showing the graphene Moiré pattern. The scale bar indicates 20 nm. (c) 50×50 nm^2 STM image, acquired in the flat central area of (b), 2D-FFT filtered to highlight the Moiré pattern. The scale bar indicates 10 nm. (d) 2D-FFT filtered STM image (acquired at V_{bias} = 0.4 V and I = 0.15 nA) showing the graphene lattice. The scale bar indicates 2 nm.

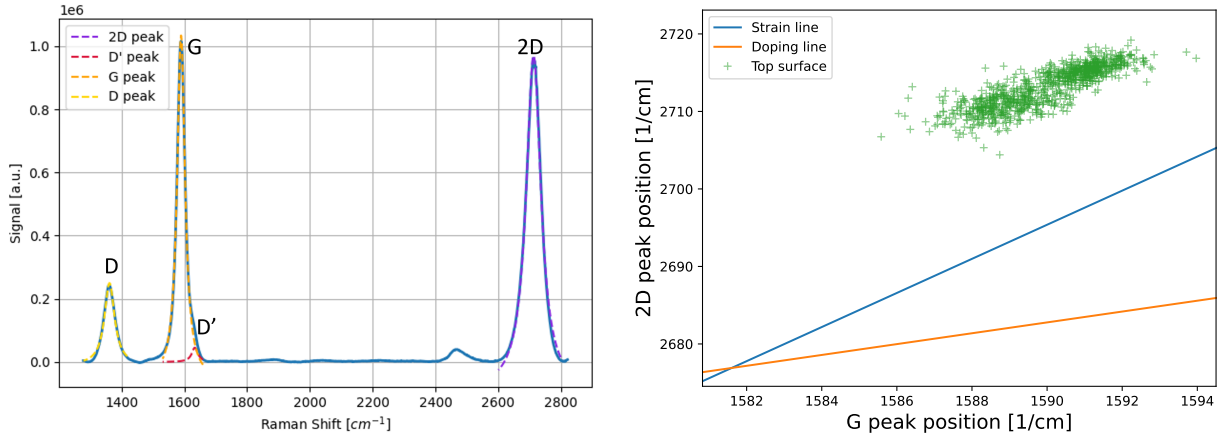

(a) (b)

FIG. S2. (a) Typical Raman spectrum of 3DG obtained by averaging over a 20×20 μm^2 Raman map. Fits of the D, G, D', and 2D peaks of graphene are shown. (b) Raman G peak position vs. 2D peak position extracted from fits of a 20×20 μm^2 Raman map acquired on a 3DG sample. The strain and the doping lines are also plotted.

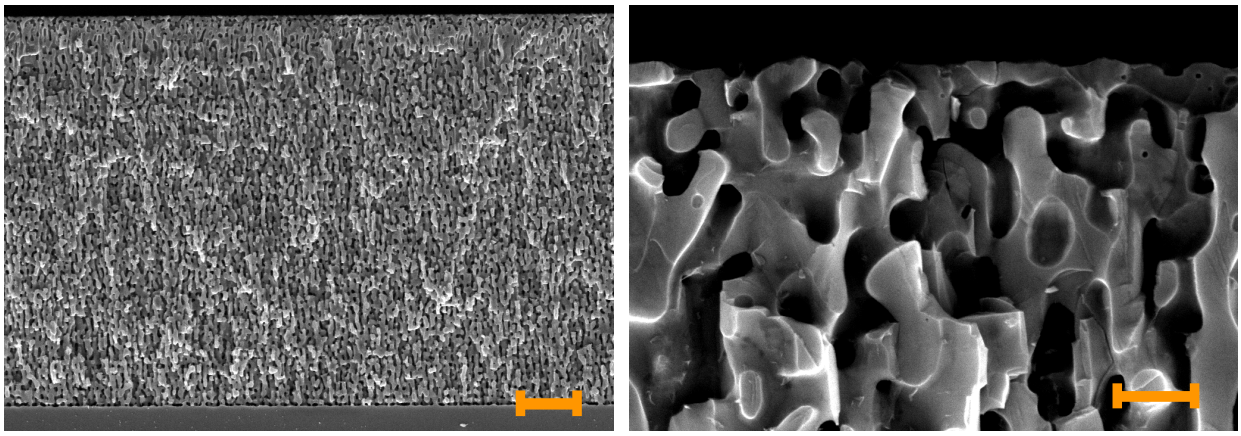

(a) (b)

FIG. S3. (a) Large scale cross-sectional SEM image showing the entire porousified layer. The scale bar indicates 3 μm. (b) Cross-sectional SEM image of the topmost region of the porousified layer. The scale bar indicates 400 nm.

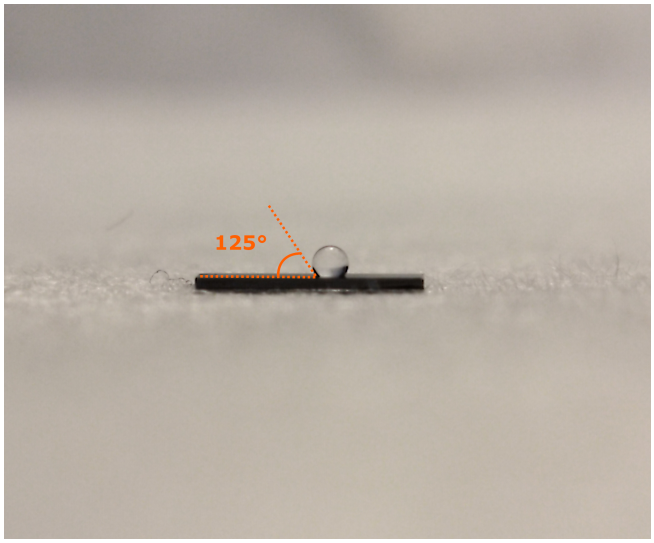

FIG. S4. Picture of a 10 μl drop of Milli-Q water deposited on the surface of a pristine 3DG sample. The hydrophobicity is evident, and the contact angle is estimated to be 125°. Analogous behavior has already been observed on similar platforms. [5]

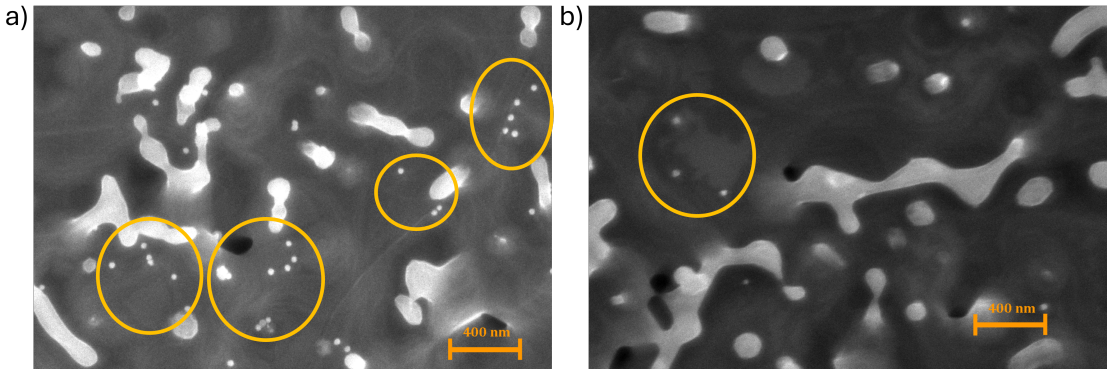

FIG. S5. SEM images of 3DG functionalized with AuNPs for 1 h under a) static condition and b) ultrasonication. NPs are visible as bright spots and have been encircled in orange. It is evident the higher density of NPs obtained in static condition.

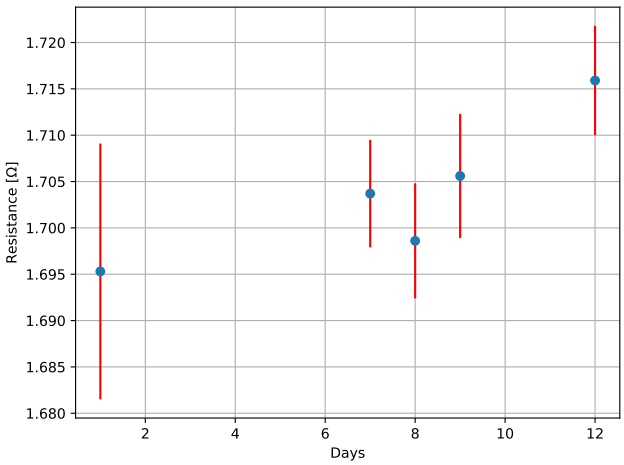

FIG. S6. Measurement of the resistance of an AuNPs-functionalized 3DG sample performed in a 4-wire configuration over many days. The value of the resistance is more than a factor 5 lower than pristine 3DG as reported in Ref. [6]

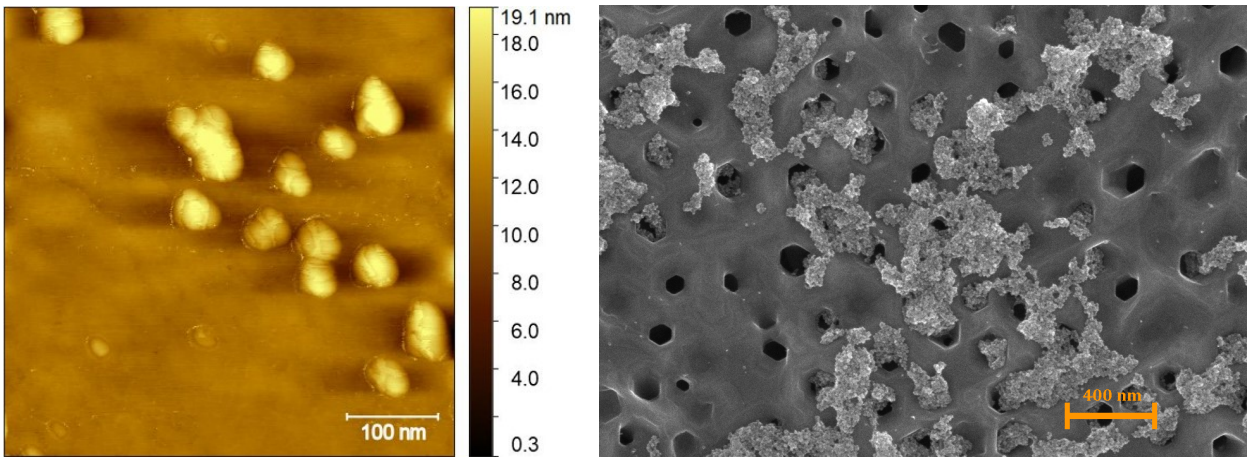

(a) (b)

FIG. S7. (a) AFM image of SDS-PdNPs deposited on a SiO_2 substrate. (b) SEM image of the surface of a SDS-PdNPs functionalized 3D graphene sample. Large PdNP clusters as well as "clean" regions are visible. Singularly dispersed NPs are not detected.

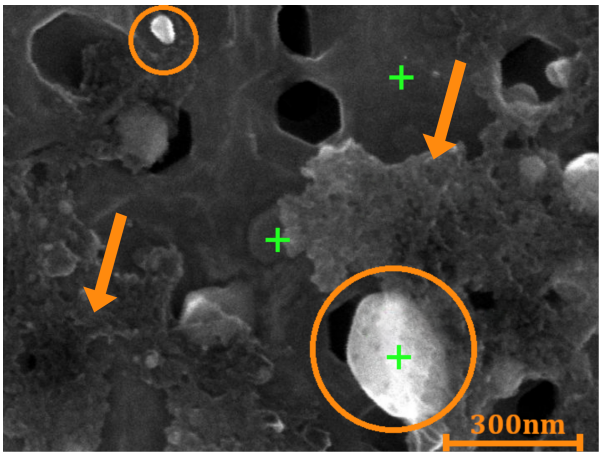

(a)

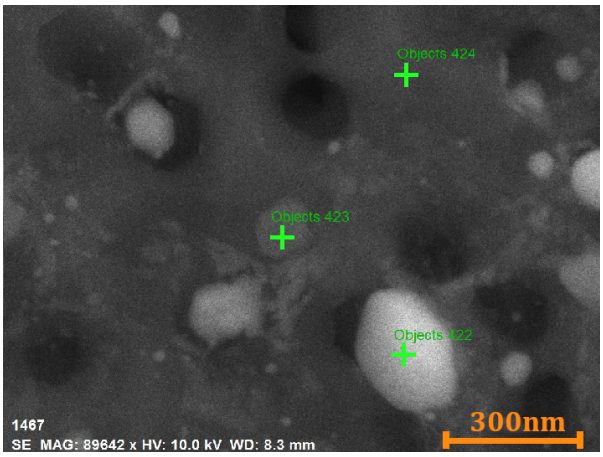

(b)

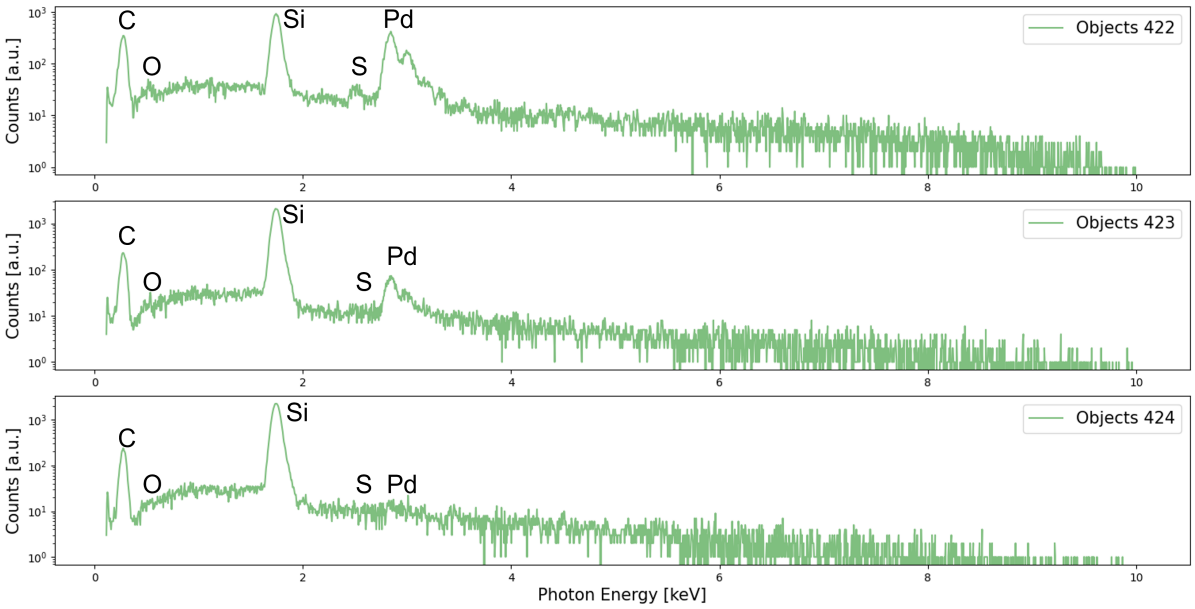

(c)

FIG. S8. (a) SEM image acquired (at 10 keV) on a 3D graphene sample functionalized with SDS-PdNPs which has been subjectet to several annealings (maximum annealing temperature was 800 °C). Large clusters of palladium are circled in orange; amorphous carbon areas are indicated by the orange arrows; the green crosses are the spots in which EDX was performed. (b) SEM image of the same region as (a) acquired utilizing the high scattering angle detector (for better visualizing palladium). Also here the EDX measurement sites are indicated by green crosses. (c) EDX spectra acquired in the three spots shown in (a) and (b). The lines of the main elements are indicated. Sulfur poisoning is detected in the spectrum acquired over the large palladium cluster (i.e., Object 422).

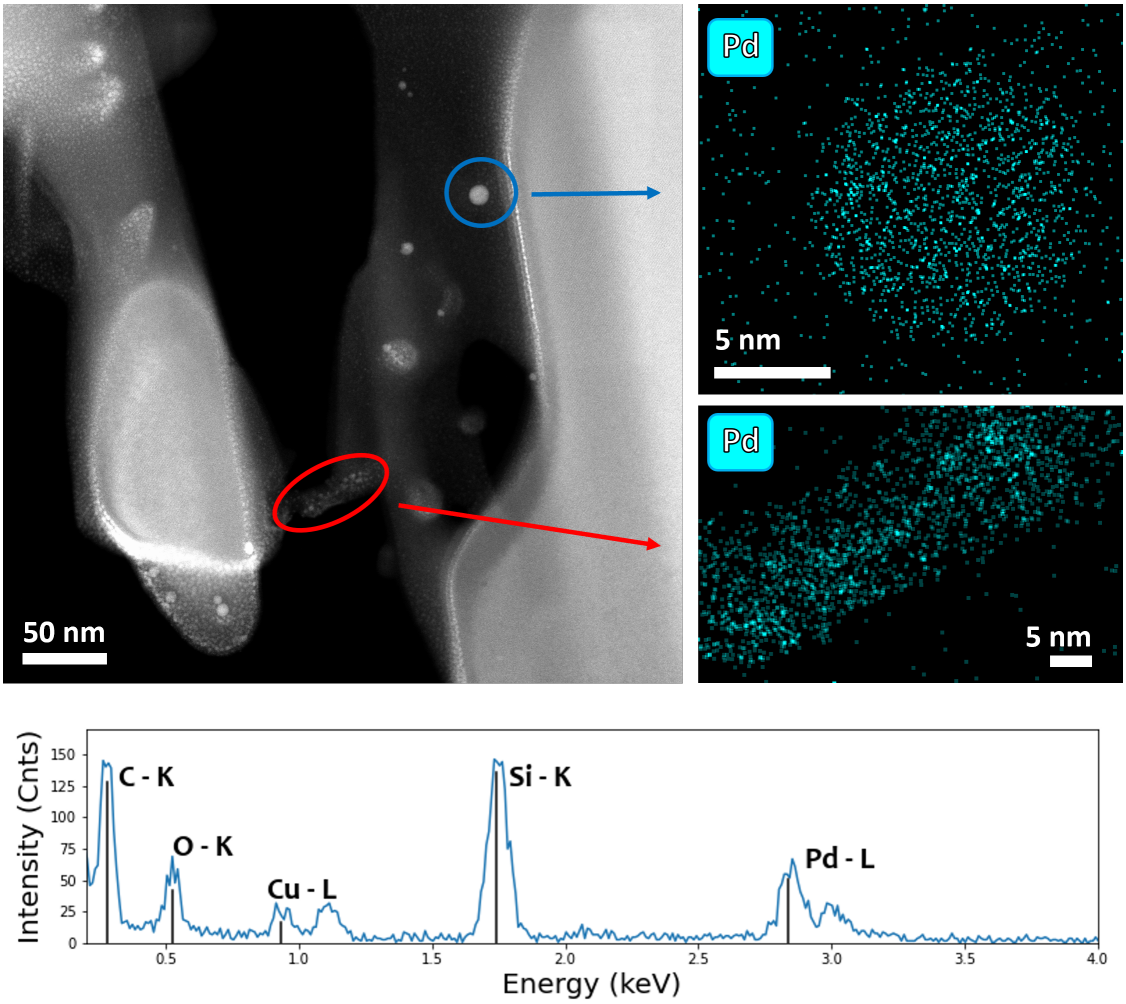

FIG. S9. Top Left: STEM cross-sectional image of a PVP-PdNPs-functionalized 3DG sample. One large PdNP is circled in blue, while a cluster of smaller NPs is circled in red. Top Right: EDX maps of palladium signal acquired in the blue and red circled regions (top and bottom image, respectively). Bottom: EDX spectrum acquired at the blue circled NP.

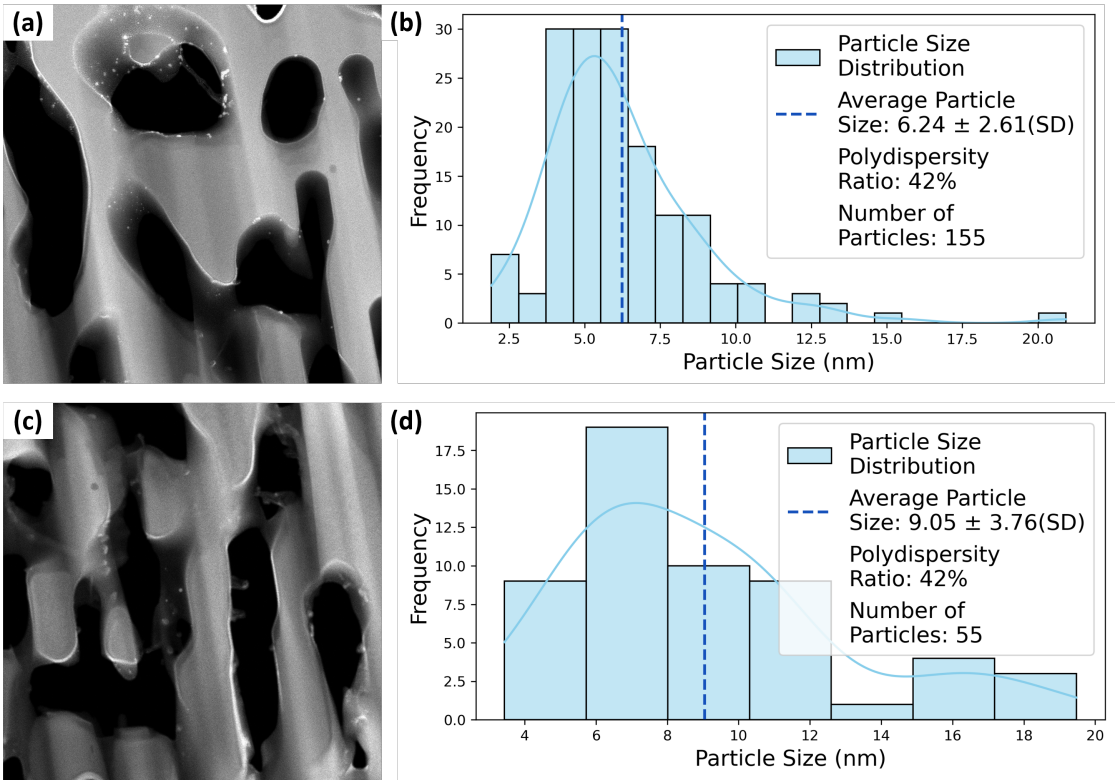

FIG. S10. HAADF TEM image of the top (a, b) and bottom (c, d) section of the thin lamella cross-section with statistical analysis of the particle size distribution.

It is fundamental to have the vast majority of the pores much larger than the size of the NPs to allow for their diffusion. Preliminary experiments performed on different samples which exhibited a reduced dimension of the pores ($\sim$ 30 nm on average) led to a negligible density of NPs deep into the porous structure. While here the pores are sufficiently large for the NPs diffusion, as demonstrated by SEM (Fig. S3) and TEM measurements (Fig. S10,S11).

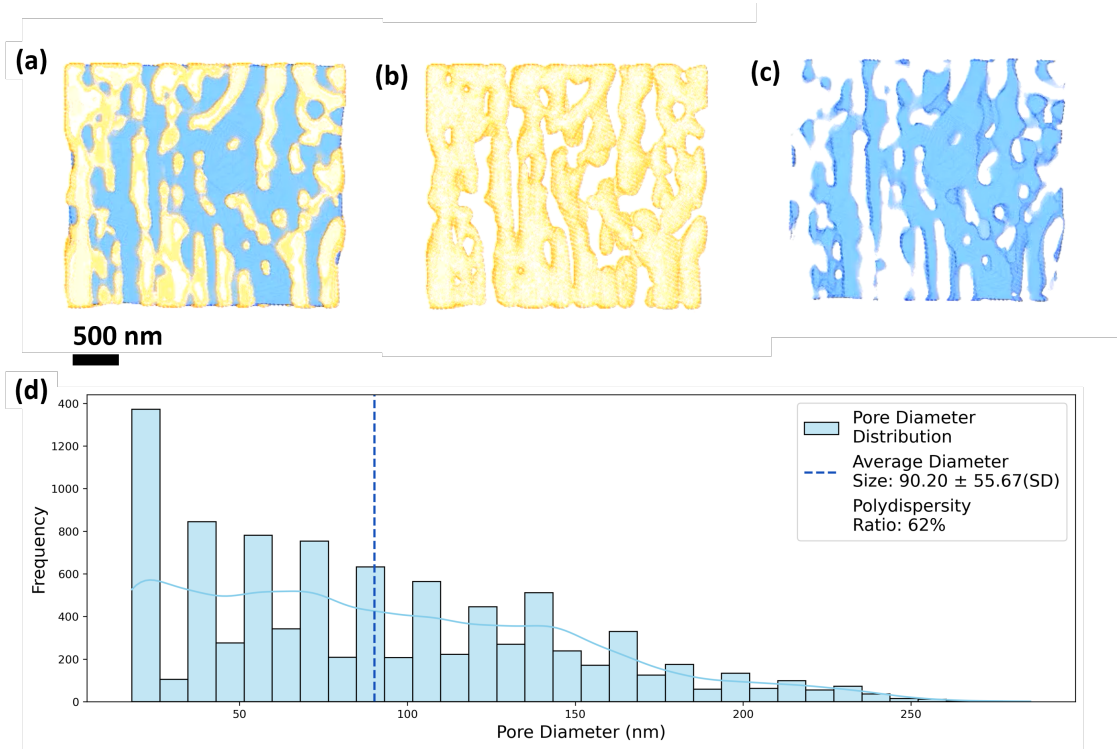

FIG. S11. Volume segmentation of the thin lamella showing the PVP-PdNPs-functionalized 3DG sample composition: (a) mix, (b) material and (c) pores. (d) statistical analysis of the pore diameter.

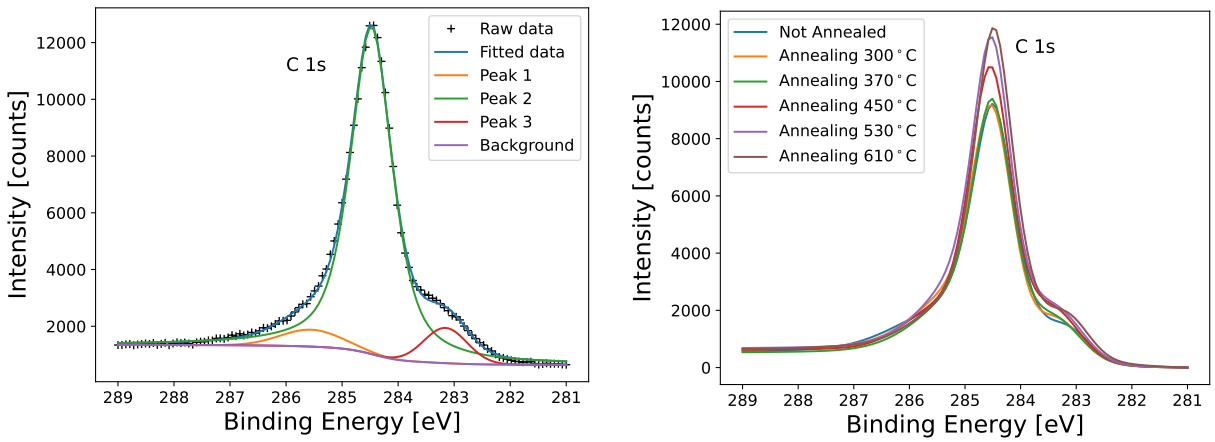

(a) (b)

FIG. S12. (a) Fit of the XPS C 1s spectrum of PVP-PdNP-functionalized 3DG after annealing at 610 °C. The fitted Shirley background signal is also plotted. The graphene buffer layer sp^3 C atoms contribute to peak 1 (285.6 eV), graphene contributes to peak 2 (284.5 eV), and SiC contributes to peak 3 (283.2 eV). (b) C 1s spectra of PVP-PdNP-functionalized 3DG acquired after each annealing step.

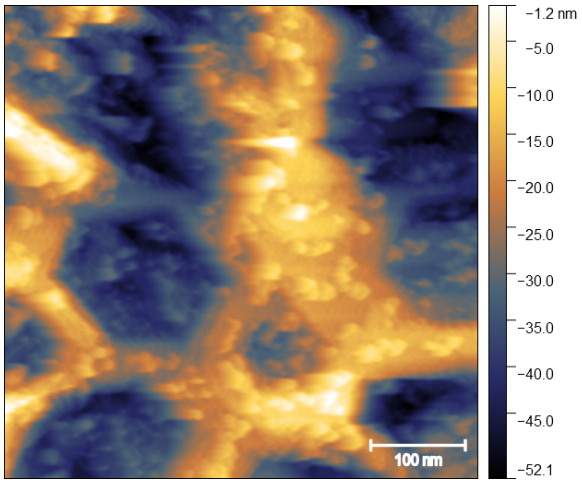

FIG. S13. 500×500 nm^2 STM image acquired (V_{bias}=1.6 V, I = 1.0 nA) on a PdNP-functionalized 3DG sample after several thermal cycles (the maximum temperature reached is 800 °C). Because of the extreme roughness of the sample surface due to the porosity and the presence of the NPs, high resolution was not achieved. However, it is possible to observe singularly dispersed NPs with diameters consistent with those of the pristine NPs (having considered the broadening due to the low resolution).

[1] A. C. Ferrari, Raman spectroscopy of graphene and graphite: Disorder, electron–phonon coupling, doping and nonadiabatic effects, Solid State Communications **143**, 47 (2007).

[2] L. G. Cançado, A. Jorio, E. H. M. Ferreira, F. Stavale, C. A. Achete, R. B. Capaz, M. V. O. Moutinho, A. Lombardo, T. S. Kulmala, and A. C. Ferrari, Quantifying Defects in Graphene via Raman Spectroscopy at Different Excitation Energies, Nano Letters **11**, 3190 (2011).

[3] J. E. Lee, G. Ahn, J. Shim, Y. S. Lee, and S. Ryu, Optical separation of mechanical strain from charge doping in graphene, Nature Communications **3**, 1024 (2012).

[4] S. Veronesi, G. Pfusterschmied, F. Fabbri, M. Leitgeb, O. Arif, D. A. Esteban, S. Bals, U. Schmid, and S. Heun, 3D arrangement of epitaxial graphene conformally grown on porousified crystalline SiC, Carbon **189**, 210 (2022).

[5] H. S. Ahn, H. Kim, J. M. Kim, S. C. Park, J. M. Kim, J. Kim, and M. H. Kim, Controllable pore size of three dimensional self-assembled foam-like graphene and its wettability, Carbon **64**, 27 (2013).

[6] S. Veronesi, Y. Vlamidis, L. Ferbel, C. Marinelli, C. Sanmartin, I. Taglieri, G. Pfusterschmied, M. Leitgeb, U. Schmid, F. Mencarelli, and S. Heun, Three-dimensional graphene on a nanoporous 4H-silicon carbide backbone: a novel material for food sensing applications, Journal of the Science of Food and Agriculture (2023).